Oil-bleeding dynamic model to predict permeability characteristics of lubricating grease

Léa Camousseigt, Aurélie Galfré, Camella Oumahi, Sandrine Muller, Melaz Tayakout-Fayolle, Françoise Couenne

Oil-Bleeding Dynamic Model to Predict Permeability Characteristics of Lubricating Grease

Léa Camousseigt [a,b*], Aurélie Galfré [a], Françoise Couenne [a], Camella Oumahi [b], Sandrine Muller [b], Melaz Tayakout-Fayolle [a]

[a] *Laboratoire d'Automatique de Génie des Procédés et de Génie Pharmaceutique (LAGEPP) at University Claude Bernard Lyon 1, Villeurbanne, F-69100, France*

[b] *Ingénierie du Matériel – Agence d'Essai ferroviaire (AEF), Société National des Chemins de Fer (SNCF), Vitry-sur-Seine, 94400, France*

** Corresponding author: leamarie.camousseigt@sncf.fr*

ABSTRACT

For grease lubrication, the dominating mechanism supplying new oil to the lubricated contact is assumed to be "oil bleeding" in which the key parameter is the grease permeability. This paper proposes a dynamic oil bleeding model based on a static oil bleeding apparatus. This model uses a permeability correlation that has been adapted to consider the effect of temperature. Grease is described as a porous network of thickener fibres that contains the oil which bleeds out when it is compressed. This system was described by mass and momentum balance equations. The resulting dynamic simulation and the experimental results were compared to obtain the permeability value by using a parametric estimation method. Results are consistent with those found in the literature.

KEYWORDS

Oil Bleeding, Microstructure Permeability, Grease Lubrication, Dynamic Modelling, Parametric estimation.

1 INTRODUCTION

Grease is a lubricant mostly used in rolling bearings. It is a two phase system composed of fluid base oil that gives its lubricant behaviour (65-97%), fibres thickener that provides its consistency (3-30%) and additives (0-5%) that protect the rolling bearings from wear or limit the grease components degradation (Lugt, 2013). From structural analyses made by Scanning Electron Microscopy (SEM) or Atomic Force Microscopy (AFM), grease thickener appears as a solid-like material of fibres with random orientation containing the oil in the free space

(Hokao et al., 2013; Mansot et al., 1989; Shuff and Clarke, 1991). In the literature, grease is considered as a colloid system for the following reasons: i) the fibres have colloidal sizes in two (more often than one) measuring directions; ii) the oil, as dispersion medium, is held in the cells of the three-dimensional grease skeleton (thickener fibres) by some adsorption bonds, and the remaining part, mechanically (Ishchuk, 2006). The role of grease is to ensure long life of the bearing and rolling element in contact with it through the formation of a lubricating film which gives low friction (Lugt, 2013). The lubricating film formation, composition and replenishment on the rolling elements have been addressed by a large number of studies in the literature. They attempted to both i) clarify the lubrication mechanisms; ii) understand the impact of operating conditions (velocity, load, grease type, temperature, etc.) on the grease life, the film thickness evolution and the rolling element's bearing life. In these studies, experiments were either carried out on specific tribological set-ups, such as ball on disc apparatus (Cann, 2006; Chapkov et al., 2007; Couronné et al., 2003; Cousseau et al., 2015; Cyriac et al., 2016), or on rolling bearings (Cann et al., 2007; Eriksson et al., 2000; Hurley et al., 2000; Morales-Espejel et al., 2014) in presence of either new or aged greases. But, due to the complexity of grease as a material, its large number of applications and the ageing of its properties, modelling of the fundamental mechanisms of grease lubricants has remained difficult. Several authors proposed that the lubricating film supplied by the oil bleeding mechanism (Eriksson et al., 2000; Lugt, 2013; Wikström and Jacobson, 1997). Grease acts as a reservoir of oil through its porous network of fibres. Thus, by applying mechanical loads such as gravity, pressure or centripetal force on grease, the oil flow passes through the thickener network. It releases from the grease and it provides lubricity onto the metallic contact area (Lugt, 2013). Oil bleeding modelling based on conservation equations has rarely been addressed in literature. To our knowledge, only Baart et al., (2010), Tichy et al., (2020), Saatchi et al., (2017) and Zhang et al., (2020) have developed a simple flow model based on Darcy's law for viscous flow in porous media for different operating conditions. Baart et al., (2010) developed a test rig under centrifugal motion to measure the film thickness evolution at different temperatures and velocities and compared their modelling results with the experimental data. Tichy et al., (2020) developed their model on a schematic view of a rolling contact filled with grease. Saatchi et al., (2017) confronted their simulation results for several greases to experimental oil bleeding rates obtained by the ASTM D6184 procedure which is similar to the NF ISO 22285:2018(F) procedure described later at the end of this section. Finally, Zhang et al. (2020) developed a model that describes the oil flow from a grease patch into a blotting paper. They consider a capillary pressure to drive the oil flow

out of the grease whereas the others authors consider pressure induced by centrifugal or gravity forces. In each study, the determination of the permeability parameter k [m^2] was required to evaluate the friction force between thickener and oil by using the Darcy law. Permeability correlations were needed to properly predict the oil bleeding rate. ***Erreur ! Source du renvoi introuvable.*** presents several correlations of permeability that we found in literature.

Table 1: Non-exhaustive table of permeability correlations seen in the literature.

Author	Permeability correlations	Notes
Gebart, (1992)	$k = \frac{2}{3}k_{per} + \frac{1}{3}k_{par}$ $k_{per} = \frac{16}{9\pi\sqrt{2}}\left(\sqrt{\frac{f_{max}}{f}} - 1\right)^{\frac{5}{2}} r^2$ $k_{par} = \frac{8}{57}\frac{(1-f)^3}{(f)^2}\ r^2$	Permeability is a summation of perpendicular and parallel contributions established in an orthogonal arrangement of fibres. f_{max} is the maximum fibre-volume fraction reached when the fibres are touching (i.e., 3π/16) and *r* is the fibre radius
Baart et al., (2010)	$k = \frac{2}{3}k_{per} + \frac{1}{3}k_{\theta}$ $k_{\theta} = \frac{k_{par}\ k_{per}}{k_{par}\ sin^2(\theta) + k_{per}\ cos^2(\theta)}$ $cos(\theta) = \frac{(f)^{-1} - (f_{max})^{-1}}{(f_0)^{-1} - (f_{max})^{-1}}$	This adds the assumption to Gebart's correlation that somefibres tilt with an angle θ. In this case, f_{max}=π/4 and θ=90° for *f*= f_{max}
Tichy et al., (2020)	$k = \frac{\varphi {D_p}^2}{32\ \tau}$	Correlation given by Happel and Brenner, (1973). This links permeability, *k* , with porosity, φ, effective pore size, D_P , and tortuosity, τ.
Saatchi et al., (2017)	$k = \frac{\varphi^5 {D_p}^2}{K}$	This is a Kozeney-type solution to model the permeability of a packed bed of randomly distributed cylinders. This uses the Kozeney constant K.

The correlation of Gebart, (1992) links the permeability to both the volume fraction and the average radius of the thickener's fibres in the grease. The fibres are assumed to all have the same cylindrical geometry (***Erreur ! Source du renvoi introuvable.***). Gebart, (1992) observed that the oil bleeding rate decreased with time because of the permeability decrease related to the increase of the fibre-volume fraction. Baart et al., (2010) modified the correlation proposed by Gebart, (1992) to include the fibres tilting during oil bleeding (***Erreur ! Source du renvoi introuvable.***). Tichy et al., (2020) used the correlation given by Happel and Brenner, (1973) which links the permeability to both the porosity and the tortuosity of the thickener network (***Erreur ! Source du renvoi introuvable.***). Finally, Saatchi et al., (2017) presented another correlation using porosity and considering the thickener as spherical floating particles in an oil matrix (***Erreur ! Source du renvoi introuvable.***) with an isotropic arrangement. Zhang et al., (2020) did not use a grease permeability correlation since they neglected it with respect to the permeability of blotting paper.

This paper presents a way to calculate the permeability by using both the modelling approach and experimental data provided by the apparatus of the NF ISO 22285:2018(F) standard procedure. In this standard test method, the oil bleeding rate is measured by applying a load to the grease. An oil-bleeding dynamic model for grease under the effect of load was built with mass and momentum balance equations for each component. The model relates the mechanical actions, the oil and thickener physical parameters, the grease porosity, and the thickener structure (through the permeability, m^2) to the one-dimensional volumetric oil flux out of the thickener porous network. The proposed model considers the deformability of the viscoelastic fibre network but also the impact of the temperature on its deformability by adding two additive parameters in the permeability correlation. For this purpose, an adaptation of the correlation of Baart et al., (2010) is proposed to consider the effect of temperature on the grease , by using a parametric estimation method at different operating temperature. The permeability parameters are estimated by fitting the simulation results for oil bleeding mass fraction versus time to the experimental data.

2 EXPERIMENTAL PART

According to ThermoGravimetric Analysis (TGA), the used grease comprises about 85 wt% of Gas-to-liquids (GTL) oil, 10 wt% of lithium hydroxystearate soap (thickener) and 5 wt% of additives. TGA consists in weighing the grease inside a furnace which is gradually increasing in temperature from 25 °C to 1000 °C. The grease components are degraded and

volatilized with the increasing temperature and, as each component has a different degradation temperature, it is possible to measure their respective mass fractions.

Erreur ! Source du renvoi introuvable. presents the density and viscosity of separated base oil and grease. It reports average results and uncertainties of each measurement because all measurements were performed three times to check the repeatability.

Table 2: Oil and grease density, viscosity and average fibres radius *Index (O, G) stand respectively for the oil and the grease.*

T	°C	25 ± 1	40 ± 1	80 ± 1
ρ_G	$kg.m^{-3}$	879.9 ± 9.4	879.4 ± 11.1	856.0 ± 11.1
ρ_O	$kg.m^{-3}$	820.7±0.1	811.2±0.1	786.7 ± 0.1
η_G	*Pa.s*	(1.15 ± 0.04) *10^{5}	(1.00 ± 0.04) *10^{5}	(8.30 ± 0.3) *10^{4}
η_O	*Pa.s*	(6.68 ± 0.06) *10^{-2}	(3.35 ± 0.04) *10^{-2}	(8.93 ± 0.06) *10^{-3}
r	*m*	(32 ± 5) *10^{-9}	(32 ± 5) *10^{-9}	(32 ± 5) *10^{-9}

The grease density was estimated by a non-standardized procedure at different temperatures. For that, grease was introduced into a graduated syringe to measure the sample volume. This syringe was placed in an oven for 2 hours to stabilize its temperature. Then, the sample mass was weighed using a precision balance of ±0.001 g.

The grease viscosity was measured with a Discovery HR-1 rheometer from TA Instruments. A low strain rate step ($5.0\ 10^{-3}\ s^{-1}$) was applied to the grease sample to measure the viscosity. The measurement was made in operating conditions as close as possible to the standard test procedure operating conditions, i.e., in the linear viscoelastic domain.

The oil density and viscosity were measured at the same time with Anton Paar viscometer SWM 3001 apparatus.

In addition to these characterisation analyses, a structural analysis was made by Scanning Electron Microscopy (SEM) to estimate the average radius of the thickener's fibres. This requires washing the grease with heptane to remove the oil and only recover the fibres. This washing step was performed two times, then the thickener network is destroyed and only the disorganised fibres remain. Several microscopy images were made (see ***Erreur ! Source du renvoi introuvable.***), and the average value of the fibres radius was calculated using the SEM software by considering a minimum of ten different fibres selected in three different areas of

the sample (see details in Appendix A). For any temperature, the average radius of the thickener's fibres (r) is about 32±5 nm (see ***Erreur ! Source du renvoi introuvable.)***.

Figure 1: Scanning Electron Microscopy (SEM) images of thickener fibres extracted from the studied grease.

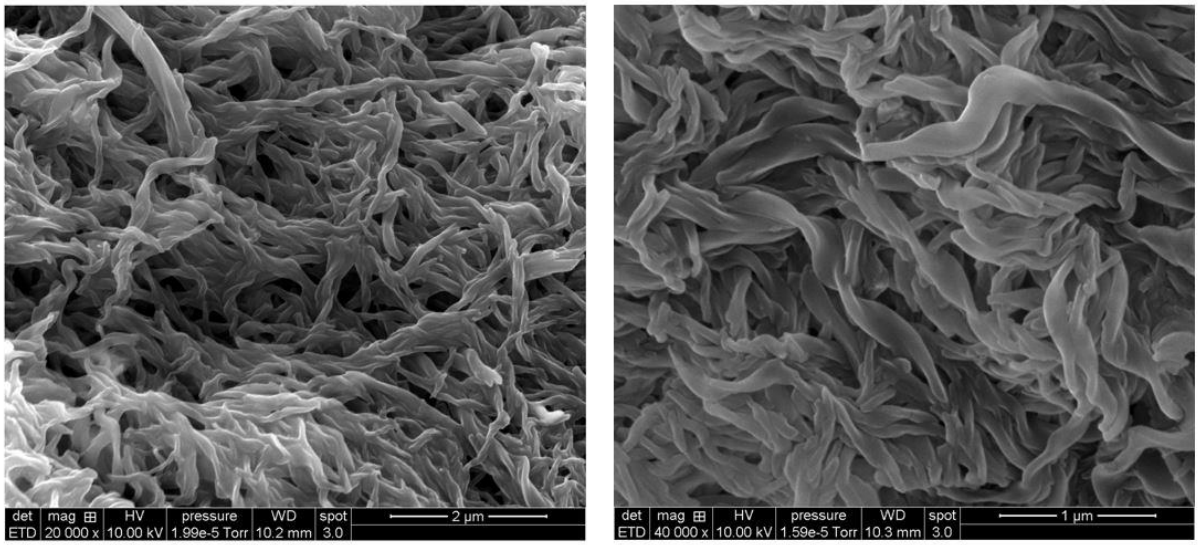

The standard test to measure the oil bleeding rate is described by the NF ISO 22285:2018(F) standard procedure. The experimental apparatus is shown in ***Erreur ! Source du renvoi introuvable.***. It is composed of a mass (a), two cylindrical chambers (b, c) and a sieve (d). The mass (a) is normalized to 100±0.1 g. The two cylindrical chamber dimensions are respectively: i) 2.05 10^{-2} m high with a diameter of 4.5 10^{-2} m for the grease chamber (b), ii) 3.5 10^{-2} m high with a diameter of 5.5 10^{-2} m for the recovered oil chamber (c). The sieve (d) has a normalized porosity of 0.32, i.e. holes cover 32 % of the total surface.

Figure 2: Apparatus according to the NF ISO 22285:2018(F) standard procedure.

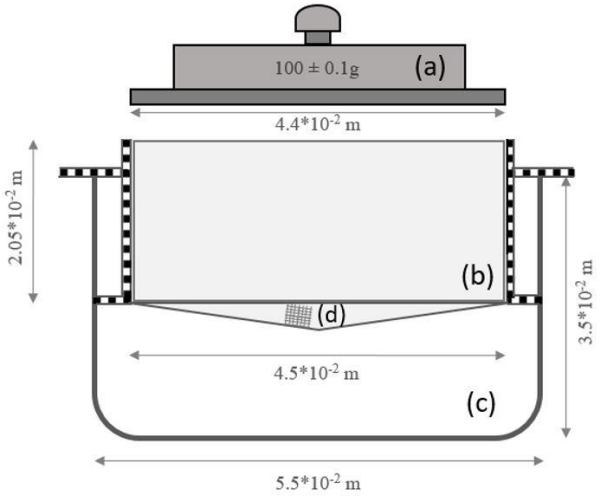

For the oil bleeding test, the experimental procedure is as follows. Three experimental tests were performed at three different temperatures according to the grease operating conditions (25, 40 and 80 °C). During the tests, the temperature was controlled and kept constant using an oven. About 32 g of grease was introduced into the cylindrical chamber (b). Before and after grease introduction, the chamber (b) was weighed to allow the grease mass to be calculated. The bleeding oil was recovered in the chamber (c). The bled oil quantity was obtained by weighing the chamber (c) at regular time intervals for 264 hours. The test time is longer than the standard duration time (168 hours according to the NF ISO 22285:2018(F) standard procedure). This time allows sufficient data to be obtained to observe the studied dynamic response whilst remaining within a reasonable experiment time.

3 MODELING PART

In this section, the dynamic oil-bleeding (1D) model, which represents the grease behaviour in the experimental standard test, is presented. ***Erreur ! Source du renvoi introuvable.*** is the 1D schematic view of the dynamic system at initial state t=0 [s] (on the left) and at time t [s] (on the right). Three subsystems are drawn in ***Erreur ! Source du renvoi introuvable.***: the "Mass" (M) with the constant height h_M [m], the "Grease" (G) with the variable height h_G (t) [m] and the "Bled Oil" with the variable height h_{BO} (t) [m].

Figure 3: One-dimensional (1D) schematic view of the system evolution under gravity and pressure forces with on the left side, the initial state (t=0 s) of the system and on the right side, state of the system at time t.

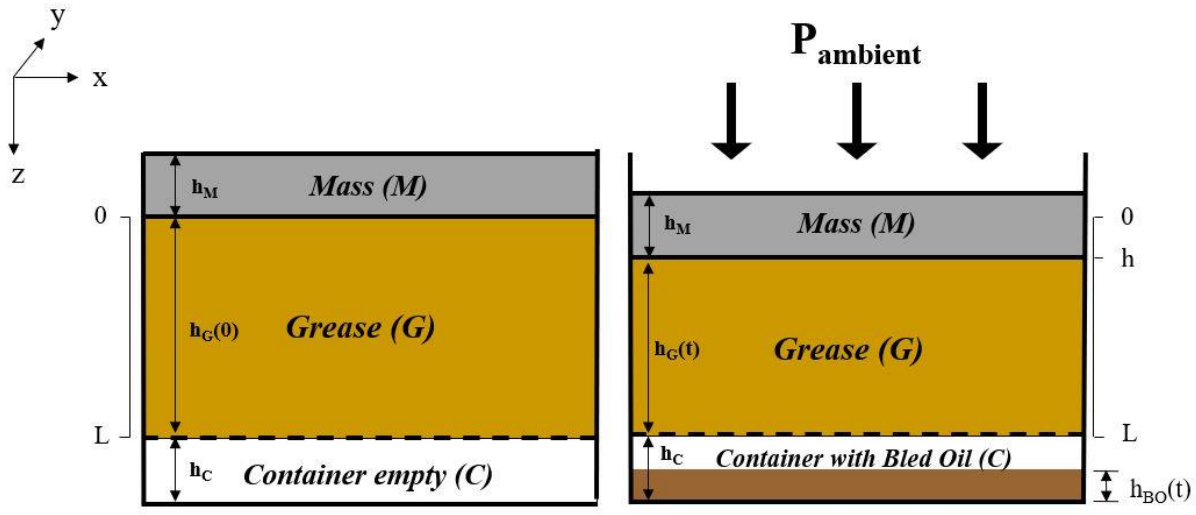

At t=0 [s], the grease (G) is held between the mass (M) at coordinate z=0 [m] and the sieve at coordinate z=L [m]. The grease height is h_G (0) = L. The oil recovery container (C) is empty and h_{BO} (t=0) = 0. At time t, the grease volume has evolved under the forces of gravity and pressure (represented by the ambient pressure $P_{ambient}$ [Pa] in the **Erreur ! Source du renvoi introuvable.**). The mass moves downwards while the grease bleeds oil through the sieve. The bled oil is recovered in the container (C).

The model is constructed of both mass and momentum balance equations, written for the grease components. These balance equations are as described by Bear, (1972) and Bird et al., (2007) and are valid in a wide range of operating conditions.

The following assumptions are made:

1. The model is one-dimensional (1D) along the z axis.
2. The chambers (b, c) and the sieve (d) (***Erreur ! Source du renvoi introuvable.***) have a constant cross-sectional area S [m^2].
3. The system is isothermal.
4. Grease is arbitrarily represented as a two-component mixture consisting of 10 wt% of thickener and 90 wt% of base oil (additives are included in the oil). In this model, it is assumed that additives have no impact on the oil properties.
5. Grease is a colloidal solution (fibres dispersed in a continuous phase which is the oil). Its behaviour can be described by a porous medium formed by solid-like material thickener fibres trapping oil as described by Bear, (1972). Indeed, under forces, the fibres stay in the grease while the oil is bleeds.
6. At time t=0 [s], the grease is uniform. Then at t>0 [s], some fibres gradually tilt with an angle θ under the forces of gravity and pressure.
7. The thickener stays in the subsystem G.
8. The oil and the thickener fibres are considered incompressible. Grease is a colloidal system whose behaviour is close to a viscous liquid. Since the shear rates are quite small, the shear thinning effects are not significant and this justifies the assumption that the grease behaves as a Newtonian fluid.. For the thickener fibres, as proposed by Tichy et al., (2020), we have assumed that the fibres are a “solid-like material”. We do not consider a particular model for the

thickener, we only assumed that they are an extremely viscous fluid whose viscosity is much higher than the liquid oil. Thickener is modelled as a generalized Newtonian fluid and oil as a Newtonian fluid. Therefore, their physical parameters (viscosity, density, …) are only dependent on temperature. Thickener properties are estimated with an ideal mixture law by using data of *Erreur ! Source du renvoi introuvable.*.

9. The oil bleeding flow through the sieve is a Poiseuille type flow as the holes of the sieve could be considered as cylinder and the oil bleeding flow could be considered as laminar flow of viscous fluid.

3.1 Notations

$d_t(-)$ stands for the time derivative of Ordinary Differential Equations (ODE). $\partial_t(-)$ and $\partial_z(-)$ stands for the time and spatial derivatives of Partial Differential Equations (PDE).

3.2 Definition of volume fraction and volumetric flow density in grease

The volumetric local flow density $f_i^G(t,z)$ [m/s] of a component i is defined as the product of the local velocity of i $v_i^G(t,z)$ [m/s] and the local volume fraction of i $\varepsilon_i^G(t,z)$ [-] (24). *i* stands for the component, oil (O) or thickener (T): $f_i^G(t,z) = v_i^G(t,z)\varepsilon_i^G(t,z)$

3.3 Momentum balance on mass M

The mass (M) is a uniform subsystem (***Erreur ! Source du renvoi introuvable.***). Then according to Bird et al., (2007), the momentum balance is written as an ODE as follows:

Momentum balance on M:

$$m_M d_t\big(v^M(t)\big) = S\big(P_{ambient} - P_G(t,h)\big) + m_M g \qquad [1]$$

In eq. [1], the right terms are pressure contribution and the gravity force, respectively.

3.4 Mass and Momentum balances of Oil and of Thickener in Grease (G)

From assumption 4, G is two component mixtures. According to Bird et al., (2007), the equation of continuity for a component in multicomponent mixture can be written as a PDE. Each component motion is done by convective flux because there is no gradient concentration.

Component i mass balance in G:

Mass balance of each component (i = T, O) can be written as follows:

$$For\ h < z < L, \qquad \partial_t\left(\varepsilon_i^G(t,z)\right) = -\partial_z\left(f_i^G(t,z)\right) \tag{2}$$

$$\text{With} \quad \varepsilon_O^G(t,z) + \varepsilon_T^G(t,z) = 1 \tag{3}$$

Global mass balance in G gives:

$$For\ h < z < L\,, \qquad \partial_z(f_O^G(t,z) + f_T^G(t,z)) = 0 \tag{4}$$

Component i momentum balance in G:

The momentum balance equations in G can be written as one PDE for each component (Bird et al., 2007). To improve the readability, *(t, z)* are omitted in the following equations [5][6].

$$For\ h < z < L,$$

$$\rho_i \partial_t\left(f_i^G\right) = -\partial_z\left(\rho_i \varepsilon_i^G \left(\frac{f_i^G}{\varepsilon_i^G}\right)^2 - \eta_i \varepsilon_i^G \partial_z\left(\frac{f_i^G}{\varepsilon_i^G}\right) + P_i^G\right) + \rho_i \varepsilon_i^G g \mp \frac{\eta_O}{k}\left(\frac{f_T^G}{\varepsilon_T^G} - \frac{f_O^G}{\varepsilon_O^G}\right) \tag{5}$$

In eq. [5], the terms on the right side are respectively the convective motion flow, the molecular momentum flux which can be written as the sum of viscous and pressure contributions, and the bulk forces (gravity force and friction force). The friction force sign $\mp$ is (-) for the thickener and (+) for the oil. The friction force is defined as in Tichy et al., (2020) and Baart et al., (2010) and according to assumption 5. This term is linked to the drag on the oil flow caused by the thickener network. It is proportional to velocity difference $\left(\frac{f_T^G}{\varepsilon_T^G} - \frac{f_O^G}{\varepsilon_O^G}\right)$, the oil viscosity η_O and inversely proportional to the permeability k. The equal and opposite force of the oil on the thickener also exists, that is why there are plus and minus signs.

Global momentum balance in G:

The sum of each component momentum balance equation using eq. [5] to evaluate the pressure term gives:

$$For\ h < z < L,$$

$$\partial_z(P_G) = -\rho_O \partial_t(f_O^G) - \rho_T \partial_t(f_T^G)$$

$$-\partial_z\left(\rho_O \varepsilon_O^G \left(\frac{f_O^G}{\varepsilon_O^G}\right)^2 + \rho_T \varepsilon_T^G \left(\frac{f_T^G}{\varepsilon_T^G}\right)^2 - \eta_O \varepsilon_O^G \partial_z\left(\frac{f_O^G}{\varepsilon_O^G}\right) - \eta_T \varepsilon_T^G \partial_z\left(\frac{f_T^G}{\varepsilon_T^G}\right)\right) \tag{6}$$

$$+\rho_O \varepsilon_O^G g + \rho_T \varepsilon_T^G g$$

3.5 Mass balance of oil in the container (C)

The bled oil (BO) (see ***Erreur ! Source du renvoi introuvable.***, on the right) is only composed of oil (assumption 7) and is also a uniform subsystem. Its equation of continuity can be written as follows.

$$d_t h_{BO}(t) = \varphi v_{grid}(t) \qquad [7]$$

In eq. [7], v_{grid} [m/s] is the oil velocity through the sieve and φ is the porosity of the sieve.

3.6 Global Mass and Momentum balances of apparatus

The mass balances for each component are also written on the total volume V_T which comprises the subsystems (G) and (C) (right side of ***Erreur ! Source du renvoi introuvable.***). In V_T, the total mass of oil M_O [kg] does not vary ($d_t(M_O) = 0$). From assumption 7, there is no thickener in the subsystem (C). Then, the total mass of thickener M_T [kg] is in G and does not vary ($d_t(M_T) = 0$).

Oil global mass balance in the volume V_T (G and C) is given by the following equation:

$$d_t(M_O) = d_t\left(\rho_O S \int_h^L \varepsilon_O^G(t,z)\,dz + \rho_O S\big(h_{BO}(t)\big)\right) = 0$$

From this equation Leibniz's formula is applied and using equation [2], two equations for oil in G are retrieved:

$$\begin{cases} f_O^G(t,h) = \varepsilon_O^G(t,h) d_t h(t) \\ f_O^G(t,L) = d_t h_{BO}(t) \end{cases}$$

Thickener global mass balance in the volume V_T (G only) is given by the following equation:

$$d_t(M_T) = \partial_t\left(\rho_T S \int_h^L \varepsilon_T^G(t,z)\,dz\right) = 0$$

By using the same approach, two equations for thickener in G are obtained:

$$\begin{cases} f_T^G(t,h) = \varepsilon_T^G(t,h) d_t h(t) \\ f_T^G(t,L) = 0 \end{cases}$$

From eqs.[3-4] and choosing $d_t h = d_t h_{BO}$ (height decrease of grease corresponds to the height increase of bleed oil) then:

$$For\ h \le z \le L,\ f_O^G(t,z) + f_T^G(t,z) = d_t h \qquad [8]$$

Global momentum balance on apparatus is given by the following equation:

$$d_t(\mathcal{P}) = P_{ambient} S - P(t,L)S + m_M g + S\int_h^L (\rho_O \varepsilon_O^G(t,z) g + \rho_T \varepsilon_T^G(t,z) g)\,dz$$

With the variation of total momentum written as follows:

$$d_t(\mathcal{P}) = d_t\left(m_M v^M(t) + \rho_O S\int_h^L f_O^G(t,z)\,dz + \rho_T S\int_h^L f_T^G(t,z)\,dz\right)$$

Using Leibniz's formula and each component momentum balance in G (i.e. eq. [5]), two equations in G are obtained to calculate the pressures $P_G(t,h)$ and $P_G(t,L)$:

$$\begin{gathered}-\rho_O \varepsilon_O^G(t,h) v_O^G(t,h)^2 + \eta_O \varepsilon_O^G(t,h)\partial_z v_O^G(t,h) \\ -\rho_T \varepsilon_T^G(t,h) v_T^G(t,h)^2 + \eta_T \varepsilon_T^G(t,h)\partial_z v_T^G(t,h) \\ \left(\rho_O f_O^G(t,h) + \rho_T f_T^G(t,h)\right)\partial_t h - P_G(t,h) + \frac{m_M}{S}\partial_t v^M(t) - P_{ambient} - \frac{m_M}{S}g = 0\end{gathered} \quad [9]$$

$$\begin{gathered}-\rho_O \varepsilon_O^G(t,L) v_O^G(t,L)^2 + \eta_O \varepsilon_O^G(t,L)\partial_z v_O^G(t,L) \\ -\rho_T \varepsilon_T^G(t,L) v_T^G(t,L)^2 + \eta_T \varepsilon_T^G(t,L)\partial_z v_T^G(t,L) - P_G(t,L) - P(t,L) = 0\end{gathered} \quad [10]$$

3.7 Pressure relation on the sieve grid

The pressure difference due to the grid holes is expressed by the Poiseuille relation (assumption 9): $\Delta P^{grid} = \frac{8\,\mu_O\,h_{grid}}{(R_{grid})^2}\left(\frac{f_O^G(t,L)}{\varepsilon_O^G(t,L)}\right)$ and the pressure at the exit of the sieve grid can be written as follows:

$$P(t,L) = \Delta P^{grid}\varphi + \left(P_{ambient} + \frac{m_M}{S}g + \rho_O g\int_h^L \varepsilon_O^G(t,z)\,dz + \rho_T g\int_h^L \varepsilon_T^G(t,z)\,dz\right) \quad [11]$$

3.8 Boundary conditions at z=h and z=L

Volume fraction ε_i^G

$$For\ i = O,T\ \ \partial_z \varepsilon_i^G(t,h) = 0 \text{ and } \partial_z \varepsilon_i^G(t,L) = 0 \quad [12]$$

Volumetric local flow density f_i^G

Assuming that the grease moves at the velocity of the mass M:

$$v^M(t) = d_t h \quad [13]$$

For oil:

$$\begin{cases} f_O^G(t,h) = \varepsilon_O^G(t,h) v^M(t) \\ f_O^G(t,L) = v^M(t) \end{cases} \quad [14]$$

For thickener:

$$\begin{cases} f_T^G(t,h) = \varepsilon_T^G(t,h)v^M \\ f_T^G(t,L) = 0 \end{cases} \quad [15]$$

3.9 Initial conditions in G

The initial state conditions are: $\forall\, z \in [h_{B0}(0), L]$

$$\varepsilon_O^G(0,z) = 0.9 \quad \text{and} \quad \varepsilon_T^G(0,z) = 0.1$$

$$f_O^G(0,z) = f_T^G(0,z) = 0$$

$$P_G(0,z) = P_{ambient}$$

3.10 Parameters

The friction force is defined as in Tichy et al., (2020). The network permeability k [m^2] correlation is the one established by Baart et al., (2010) (***Erreur ! Source du renvoi introuvable.***) but modified here. In the works of Baart et al., (2010), the permeability is not temperature dependent. In this work, the adjustment constants C_{par}^{te} and C_{per}^{te} are added to consider the fibres and network defects and to evaluate the effect of temperature. The correlation is as follows:

$$k = \frac{2}{3}k_{per} + \frac{1}{3}k_{\theta} \quad [16]$$

Where the coefficients (2/3 and 1/3) are for an isotropic distribution of the fibers.

With:

$$k_{per} = C_{per}^{te} \frac{16}{9\pi\sqrt{2}} \left(\sqrt{\frac{\varepsilon_{T,max}^G}{\varepsilon_T^G}} - 1 \right)^{5/2} r^2 \quad [17]$$

$$k_{par} = C_{par}^{te} \frac{8}{57} \frac{(1-\varepsilon_T^G)^3}{(\varepsilon_T^G)^2} r^2 \quad [18]$$

$$k_{\theta} = \frac{k_{par}\, k_{per}}{k_{par}\, sin^2(\theta) + k_{per}\, cos^2(\theta)} \quad [19]$$

$$cos(\theta) = \frac{h_G(t) - h_{G,min}}{h_G(0) - h_{G,min}} = \frac{\left(\varepsilon_T^G(t,z)\right)^{-1} - \left(\varepsilon_{T,max}^G\right)^{-1}}{\left(\varepsilon_T^G(0,z)\right)^{-1} - \left(\varepsilon_{T,max}^G\right)^{-1}} \quad [20]$$

$\varepsilon_{T,max}^G$ is the maximum fibre volume fraction reached when the fibres are in contact. Its value remains unchanged from Baart et al., (2010) work, i.e. $\varepsilon_{T,max}^G = \pi/4$.

The equation [19] shows that the bounds of k_θ are k_{par} and k_{per} when θ is respectively equal to 0° or 90°. Moreover for θ=90°, $\varepsilon_T^G(t,z)$ finally becomes $\varepsilon_{T,max}^G$ and the oil bleeding stops as the permeability becomes zero considering eqs [16] and [17].

And, using an ideal mixture law (see Tichy et al., (2020) and Bird et al., (2007)), the viscosity η (assumption 8) and density ρ of thickener are as follows:

$$\eta_T = \frac{(\eta_G - \varepsilon_O^G\, \eta_O)}{\varepsilon_T^G} \; and \; \rho_T = \frac{(\rho_G - \varepsilon_O^G\, \rho_O)}{\varepsilon_T^G} \qquad [21]$$

3.11 Numerical simulation of the oil bleeding model

The computer code was developed in MATLAB® (R2019b 9.7.0.) software. The set of PDEs (see ***Erreur ! Source du renvoi introuvable.)*** was reduced to a set of ODEs by applying the finite difference method to the spatial coordinate for the grease. The grease height is being discretised into *N* infinitesimal elements, the step size Δz is calculated at each integration time as follows:

$$\Delta z = \frac{L-h}{N+1}$$

The numerical model was composed of 2N+1 variables described by ODEs ($\varepsilon_T^G(t,z)$,$f_T^G(t,z)$,$h_{BO}(t)$, $v^M(t)$, $h(t)$) and N+6 algebraic constraints ($P_G(t,z)$, $\varepsilon_T^G(t,h)$,$f_T^G(t,h)$, $\varepsilon_T^G(t,L)$,$f_T^G(t,L)$) (see *Erreur ! Source du renvoi introuvable.* for details). The list of the variables and their associating equations is presented in ***Erreur ! Source du renvoi introuvable.***. The resulting ordinary differential-algebraic system of equations was solved using the MATLAB integration subroutine (ODE15i function).

Table 3: List of the model's variables and their associating equations

Variable	Type of the associating equation	Number of the associating equation
$For\ i = O,T$ $For\ h < z < L\ \varepsilon_i^G(t,z)$	Mass balances on G	[2] and [3]
$For\ i = O,T$ $\varepsilon_i^G(t,h)\ and\ \varepsilon_i^G(t,L)$	Boundary conditions	[12] and [3]
$For\ i = O,T$ $For\ h < z < L\ f_i^G(t,z)$	Momentum balances on G	[5] and [8]

$f_O^G(t,h)\ and\ f_O^G(t,L)$	Boundary conditions	[14]
$f_T^G(t,h)\ and\ f_T^G(t,L)$	Boundary conditions	[15]
$For\ h < z < L\ P_G(t,z)$	Global momentum balances on G	[6]
$P_G(t,h)\ and\ P_G(t,L)$	Global momentum balance of apparatus	[9] and [10]
$P(t,L)$	Forces balance equation	[11]
$v^M(t)$	Momentum balance on M	[1]
$h_{BO}(t)$	Mass balance on C	[7]
$h(t)$	Boundary conditions	[13]

3.12 Parameters' estimation of the oil bleeding model

The grease permeability k [m²] depends on the adjustment constants C_{par}^{te} and C_{per}^{te} of eqs. [17] and [18]. These constant parameters were estimated by a Levenberg–Marquardt procedure (see Marquardt, (1963)). The aim is to minimize the sum of the squared errors between experimental and simulated results of the bleeding oil mass fraction with respect to the parameters. The MATLAB function "lsqnonlin" is used for this purpose. The confidence intervals of the estimated parameters were calculated using standard procedure (see Beck and Arnold, (1977)). Errors associated with two successive measurements were independent, centred and followed a normal distribution.

The equations for the confidence intervals are as follows:

$$\bar{k} - t_{student}\sqrt{H\sigma^2} < k < \bar{k} + t_{student}\sqrt{H\sigma^2}$$

Where $\bar{k}$ is the estimate of *k*, *H* is the Hessian matrix, σ^2 is the variance estimator of experimental measurements and $t_{student}$ is the student variable.

The Hessian Matrix *H=J'*J* was calculated by using the numerical evaluation of the jacobian matrix J (sensitivity matrix) given by the "lsqnonlin" function of MATLAB.

4 RESULTS AND DISCUSSION

In the following part, all the figures present results at three temperatures (25, 40 and 80 °C). *Erreur ! Source du renvoi introuvable.* exhibits the estimated adjustment constants (C_{par}^{te} and C_{per}^{te}) and their dependence laws versus temperature. **Erreur ! Source du renvoi**

introuvable., **Erreur ! Source du renvoi introuvable.** and ***Erreur ! Source du renvoi introuvable.*** show the evolution of the bleeding oil mass fraction, the mass (M) displacement velocity, and the thickener fibres deviation angle versus time respectively. And finally, ***Erreur ! Source du renvoi introuvable.*** presents the local permeability (k) with its three contributions (k_{per}, k_{par} and k_{θ}) versus the thickener fibres deviation angle.

Erreur ! Source du renvoi introuvable. presents the estimated adjustment constants (C_{par}^{te} and C_{per}^{te}) and their confidence intervals at 95 % for three temperatures. C_{par}^{te} and C_{per}^{te} are statistically significant with low confidence intervals. C_{par}^{te} is more sensitive than C_{per}^{te}. Two temperature dependence laws, valid in the range 25 °C and 80 °C, were estimated to express these two different relations as follows (*Erreur ! Source du renvoi introuvable.)*:

$$C_{par}^{te} = = 56300\left(1 - e^{(-0.07\ (T-24.9))}\right) \quad [22]$$

$$C_{per}^{te} = 24.5\left(1 - e^{(-0.08\ (T-19))}\right) \quad [23]$$

Both C_{par}^{te} and C_{per}^{te} are more temperature sensitive in the range from 25 °C to 40 °C and less so above 40°C. The temperature increase expands the thickener network, probably by increasing the mobility of the fibres. The C_{par}^{te} and C_{per}^{te} asymptotic values correspond to the maximum rate to reach a given equilibrium position of the fibres in the network, which no longer move. This probably also corresponds to the maximum fibre volume fraction ($\varepsilon_{T,max}^{G}$) reached when the fibres are in contact as described by Baart et al., (2010).
The higher temperature sensitivity of C_{par}^{te} can be related to the shape factor (c) used in the correlation of k_{par} designed by Gebart, (1992). This shape factor is inversely proportional to k_{par} and decreases as the flow cross section increases with the expansion of the network.

Figure 4: Modelling results: evolution of the estimated permeability adjustment constants versus temperature.

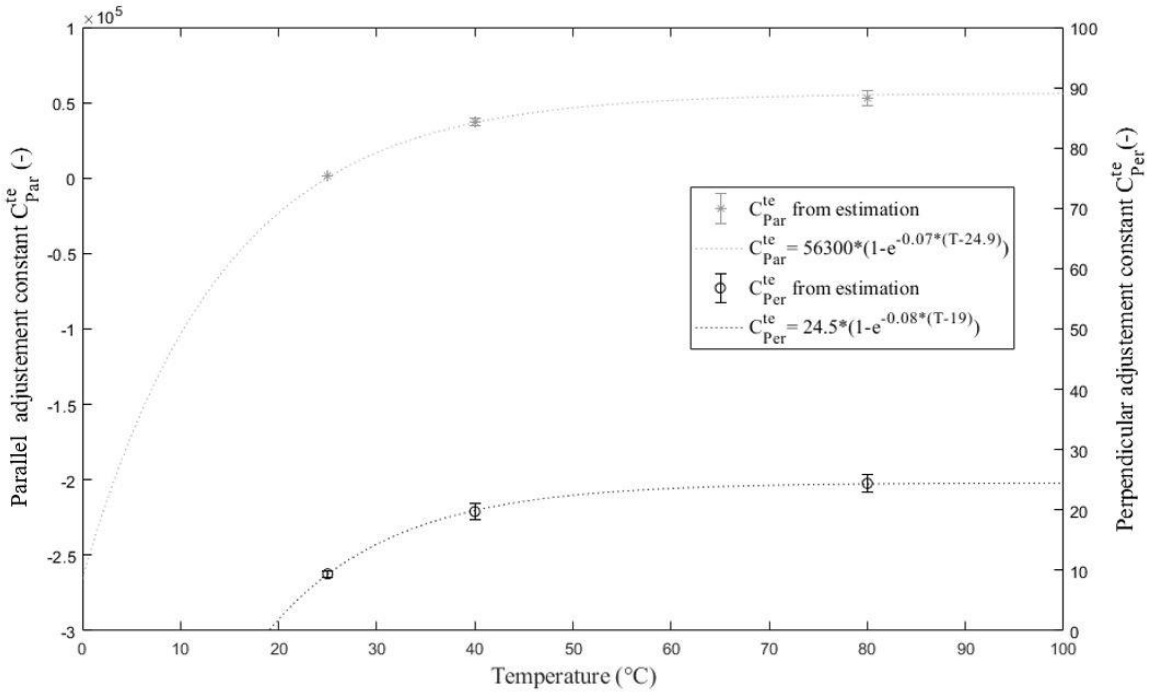

Erreur ! Source du renvoi introuvable. indicates good agreement between the experiments and the model results using the estimated adjustment constants C_{per}^{te} and C_{par}^{te} (*Erreur ! Source du renvoi introuvable.*) for each temperature. **Erreur ! Source du renvoi introuvable.** also reveals that the steady state of the system is still not reached at 400 h. The simulation was used to predict this steady state and the obtained values of time, bleeding oil mass fraction and thickener fibres deviation angle were listed in *Erreur ! Source du renvoi introuvable.*.

Figure 5: Modelling results: evolution of the oil bleeding weight percent versus time. Dots: experimental data at 25, 40 and 80°C. Lines: modelling results at 25, 40 and 80°C.

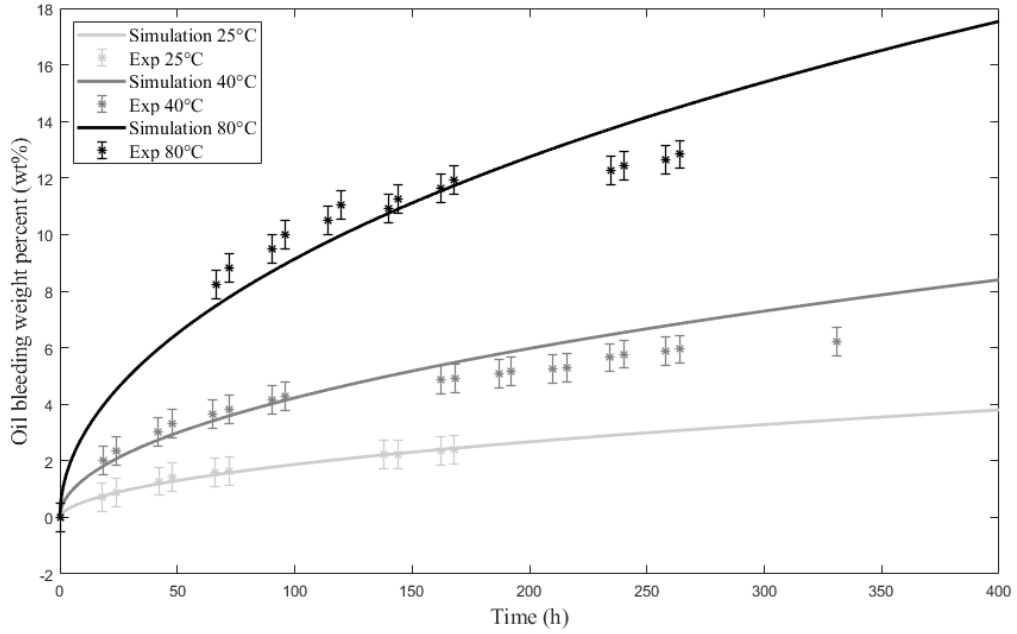

Table 4: Modelling results: steady state values of time, oil bleeding mass fraction and thickener fibres deviation angle at different temperatures.

T	°C	25 ± 1	40 ± 1	80 ± 1
t	year	110	25	7
Bleed oil	wt.%	58	58	58
θ	Degree	67	67	67

The higher the temperature is, the faster the oil bleeding is. This is due to the increases of the permeability value with temperature as shown in ***Erreur ! Source du renvoi introuvable.***.

From **Erreur ! Source du renvoi introuvable.**, the velocity of mass (M) displacement appears to increase to a maximum during the first 2 hours (zoom window in **Erreur ! Source du renvoi introuvable.**) before gradually decreasing. The initial increase is very clear in the data measured at 25°C and is visible at 40°C. In **Erreur ! Source du renvoi introuvable.**, we distinguished two distinct time evolutions which we describe here as follows.

- At the initial moment (t < 2h), positioning the mass (M) on the grease acts as a system disruption which induces a high mass (M) displacement velocity (zoom window in **Erreur ! Source du renvoi introuvable.**). Indeed, the grease responds to this disruption by a quick rearrangement of the fibres that tilt with the deviation angle shown in ***Erreur ! Source du renvoi introuvable.***. The time variation of the thickener fibres deviation angle is a function of the temperature: the higher the temperature is, the greater the deviation angle variation is. This is linked to the friction force, which is lower at higher temperature because of its dependence on oil viscosity and permeability.
- For t >2h, there is a stabilization of the system disruption and the mass (M) displacement velocity (**Erreur ! Source du renvoi introuvable.**), and the time variation of the deviation angle (***Erreur ! Source du renvoi introuvable.)***, decreases. The pattern of this second evolution seems to be less temperature dependent than the preceding behaviour

Figure 6: Modelling results: evolution of the mass displacement velocity (v^M) versus time at different temperatures.

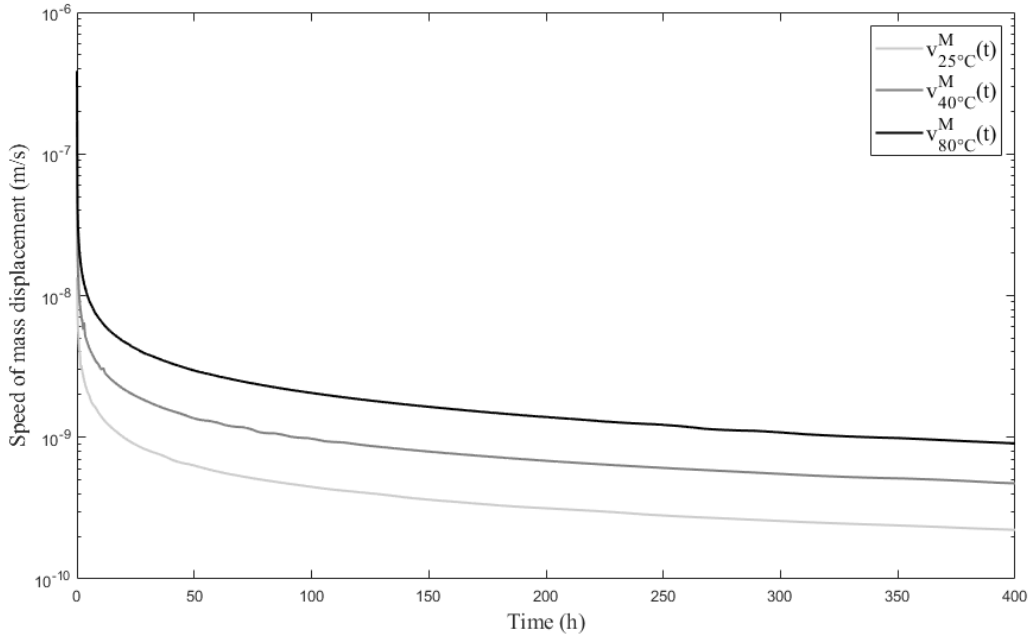

Figure 7: Modelling results: evolution of the thickener fibres deviation angle (θ) versus time at different temperatures.

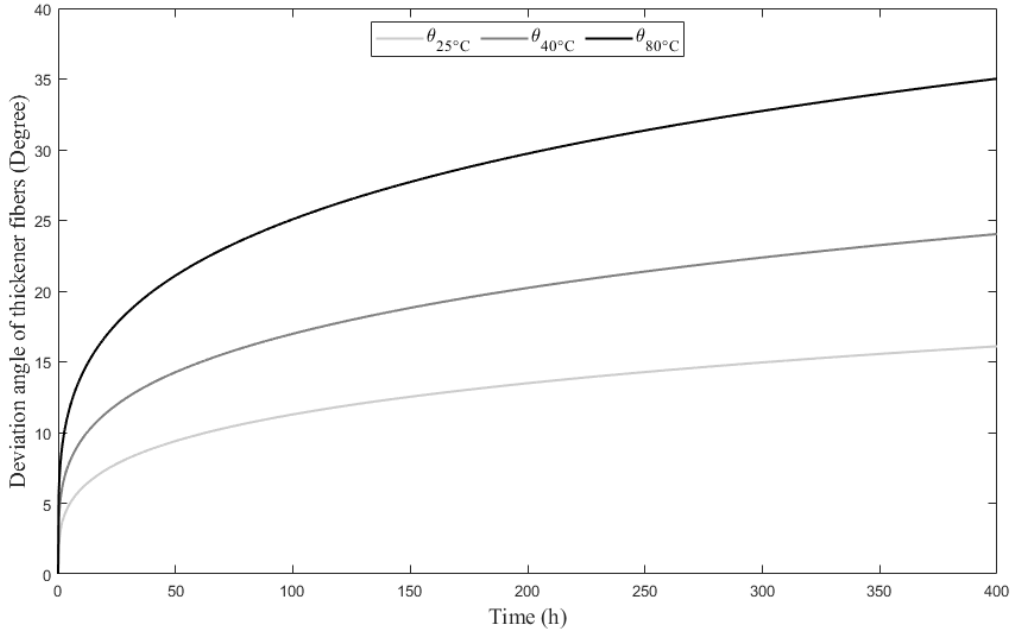

Erreur ! Source du renvoi introuvable. shows that k_θ starts from k_{par} and gradually goes to k_{per}, as expected, and as k_{par} depends strongly on temperature, the permeability (k) increases with temperature.

Figure 8: Modelling results: evolution of local permeability (k) and its three contributions (k_{per}, k_{par} and k_θ) versus thickener fibres deviation angle of at different temperatures.

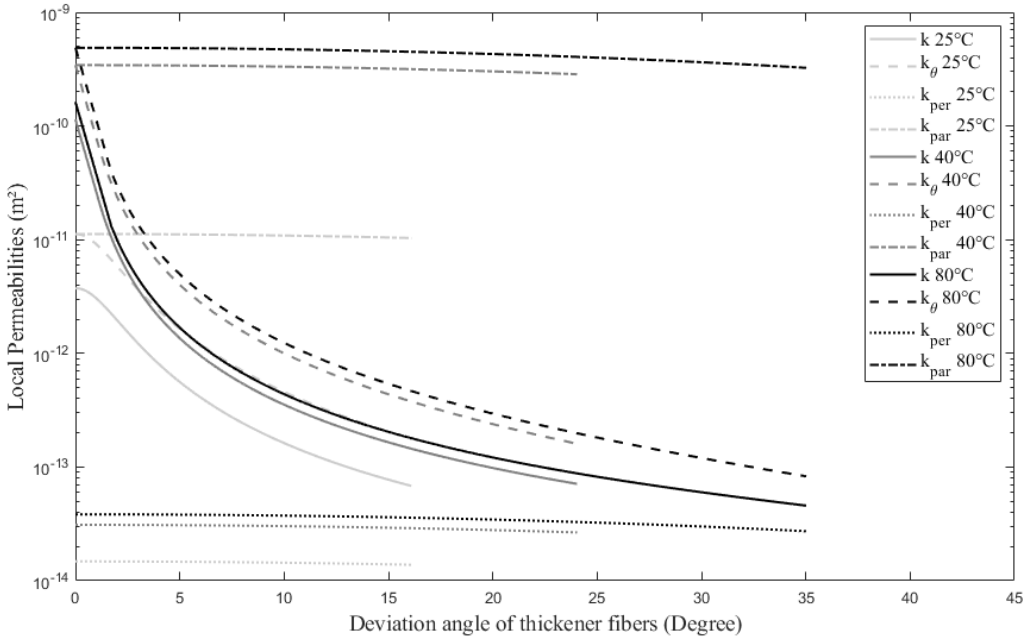

It is difficult to compare our results with the works of the authors listed in ***Table 1*** because they were performed in rotating apparatus and the grease properties were totally different. Only the following conclusions could be made:

- Baart et al., (2010) work on a similar grease (with lithium soap) and obtain results for a different range of volume fraction of thickener ($\varepsilon_T^G > 0{,}2$) because they consider more powerful bulk forces (centrifugal force). Thus, our respective permeability results are not directly comparable. However, if we extrapolate Baart's results to a lower volume fraction of thickener, our values are in the same range ($10^{-15}m^2 \leq k \leq 10^{-13}m^2$).
- Baart et al., (2010) propose an intrinsic correlation of permeability without taking temperature into account. This paper adds an empirical parameter of temperature dependence to their correlation.

5 CONCLUSIONS

A dynamic oil-bleeding model for grease under load in a static apparatus is proposed. Grease is considered as a two-component mixture consisting of 10 wt% thickener (lithium hydroxystearate soap) and 90 wt% of GTL oil (including non-impacting additives). In this

case, it can be described as a porous medium formed by thickener fibres floating in oil. The objective of this work was to develop a model able to estimate the grease permeability parameter as intrinsically as possible and hence, predict grease oil bleeding over time in a static apparatus under gravity and pressure. The system considered has been designed to correspond to the static oil bleeding standard procedure (reference NF ISO 22285:2018(F)). As a first approximation, this model was developed in one dimension and the temperature is assumed to be constant and uniform.

The model equations are based on mass and momentum balances. Finite differences and boundary conditions were used to allow the equations to be solved numerically in MATLAB. The resulting simulation was compared to experimental results from the static oil bleeding standard procedure. Finally, a parametric estimation method was used to obtain the permeability value associated with the grease studied under the experimental operating conditions.

The permeability has been studied for three temperatures according to the grease operating conditions (25, 40 and 80 °C). In addition, a semi-empirical permeability correlation was designed by adapting an intrinsic correlation (Baart et al., 2010) to take into account the influence of temperature. Two conclusions were drawn. First, and as expected, permeability increases with temperature. Second, the permeability correlation proposed in this paper gives values consistent with those given in the literature (Baart et al., 2010). Finally, each grease can have a different thickener geometry (different particles, differently oriented fibres, etc.): the permeability correlation has to be chosen on a case-by-case basis according to the thickener structure.

The model could be further developed for this apparatus in many ways. For example, by extension to 3D flows, non-Newtonian flow, mechanical or chemical aging of the grease, etc. Furthermore, additional problems could be considered, such as adding the effect of the centripetal force to better represent the operating conditions of rolling bearings or considering the non-isothermal behaviour of the system which requires including the energy balance equations. However, the present model is a first step to understand modelling of the grease lubricating physical mechanisms.

6 ACKNOWLEDGMENTS

The work described in this article was conducted at the Railway Testing Agency of the Rolling Stock Engineering Department of SNCF Voyageurs (AEF-SNCF) and LAGEPP. The

authors thank the AEF-SNCF team and the LAGEPP's DYCOP team for valuable discussion on these topics. They thank more particularly the AEF-SNCF team for its funding and experimental support and the LAGEPP's DYCOP team for its modelling and numerical simulation support.

The Authors are particularly grateful to Melha Khaleche who performed all the experimental oil bleeding measurements at SNCF.

7 APPENDICES

Appendix A: Estimation of the average radius of the thickener's fibres

SEM images of thickener fibres extracted from the grease of the 25°C experiment.

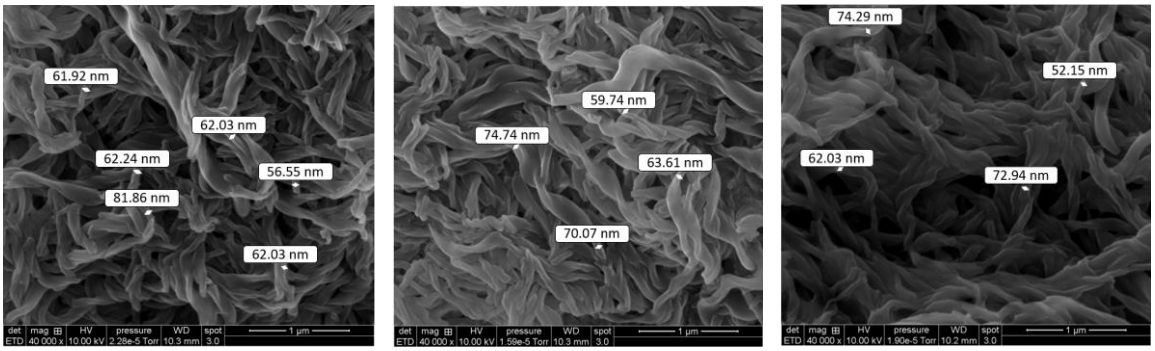

SEM images of thickener fibres extracted from the grease of the 40°C experiment.

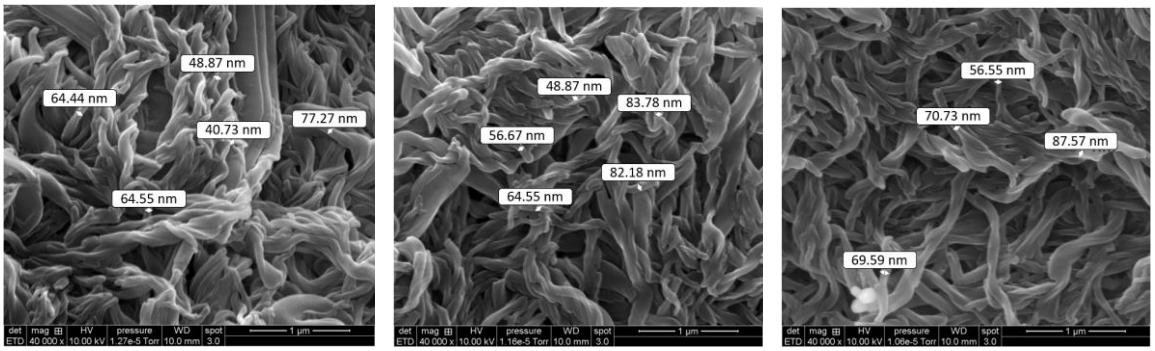

SEM images of thickener fibres extracted from the grease of the 80°C experiment.

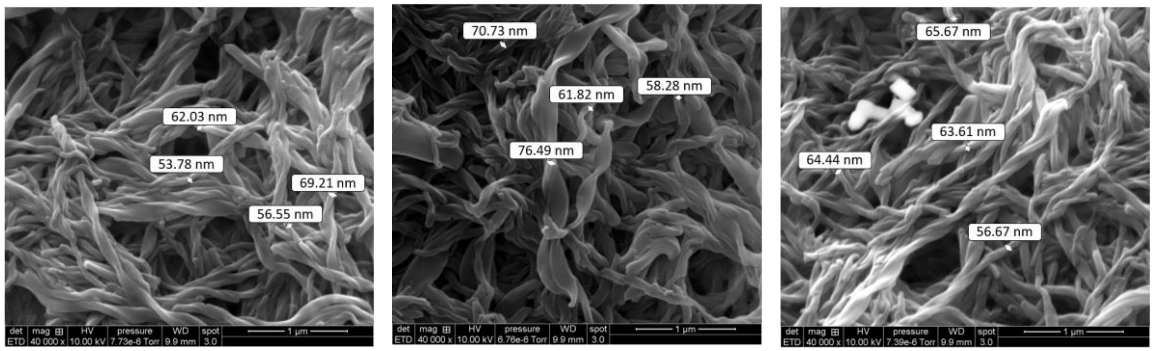

8 REFERENCES

Baart, P., van der Vorst, B., Lugt, P.M., van Ostayen, R.A.J., 2010. Oil-Bleeding Model for Lubricating Grease Based on Viscous Flow Through a Porous Microstructure. Tribol. Trans. 53, 340–348. https://doi.org/10.1080/10402000903283326

Bear, J., 1972. Dynamics of Fluids in Porous Media, Dover Publications. ed.

Beck, J.V., Arnold, J., 1977. Parameter estimation in Engineering and Science, John Wiley & Sons Inc.

Bird, R.B., Stewart, W.E., Lightfoot, E.N., 2007. Transport phenomena, Rev. 2. ed. ed. Wiley, New York.

Cann, P.M., 2006. Grease degradation in a bearing simulation device. Tribol. Int. 39, 1698–1706. https://doi.org/10.1016/j.triboint.2006.01.029

Cann, P.M., Webster, M.N., Doner, J.P., Wikstrom, V., Lugt, P., 2007. Grease Degradation in R0F Bearing Tests. Tribol. Trans. 50, 187–197. https://doi.org/10.1080/10402000701261003

Chapkov, A.D., Bair, S., Cann, P., Lubrecht, A.A., 2007. Film thickness in point contacts under generalized Newtonian EHL conditions: Numerical and experimental analysis. Tribol. Int. 40, 1474–1478. https://doi.org/10.1016/j.triboint.2007.01.002

Couronné, I., Vergne, P., Mazuyer, D., Truong-Dinh, N., Girodin, D., 2003. Effects of Grease Composition and Structure on Film Thickness in Rolling Contact. Tribol. Trans. 46, 31–36. https://doi.org/10.1080/10402000308982596

Cousseau, T., Graça, B., Campos, A., Seabra, J., 2015. Grease Aging Effects on Film Formation under Fully-Flooded and Starved Lubrication. Lubricants 3, 197–221. https://doi.org/10.3390/lubricants3020197

Cyriac, F., Lugt, P.M., Bosman, R., Padberg, C.J., Venner, C.H., 2016. Effect of Thickener Particle Geometry and Concentration on the Grease EHL Film Thickness at Medium Speeds. Tribol. Lett. 61, 18. https://doi.org/10.1007/s11249-015-0633-z

Eriksson, P., Wikström, V., Larsson, R., 2000. Grease passing through an elastohydrodynamic contact under pure rolling conditions. Proc. Inst. Mech. Eng. Part J J. Eng. Tribol. 214, 309–316. https://doi.org/10.1243/1350650001543197

Gebart, B.R., 1992. Permeability of unidirectional reinforcements for RTM. J. Compos. Mater. 26.

Happel, J., Brenner, H., 1973. Low Reynolds number hydrodynamics. Noordhoff Int.

Hokao, M., Inami, N., Watabe, E., Yokouchi, A., Sugimura, J., 2013. A study of the structure formed by thickeners of greases using atomic force microscope. Tribol. Online 8, 76–82.

Hurley, S., Cann, P.M., Spikes, H.A., 2000. Lubrication and Reflow Properties of Thermally Aged Greases. Tribol. Trans. 43, 221–228. https://doi.org/10.1080/10402000008982332

Ishchuk, Y.L., 2006. Lubricating Grease Manufacturing Technology. New Age Int. P Ltd Publ. New Delhi.

Lugt, P.M., 2013. Grease lubrication in rolling bearings, John Wiley&Sons. ed.

Mansot, J.L., Terech, P., Martin, J.M., 1989. Structural investigation of lubricating greases. Colloids Surf. 39, 321–333.

Marquart, D., 1963. An Algorithm for Least-squares Estimation of Nonlinear Parameters. SIAM J. Appl. Math. 11, 431–441.

Morales-Espejel, G.E., Lugt, P.M., Pasaribu, H.R., Cen, H., 2014. Film thickness in grease lubricated slow rotating rolling bearings. Tribol. Int. 74, 7–19. https://doi.org/10.1016/j.triboint.2014.01.023

Saatchi, A., Shiller, P.J., Eghtesadi, S.A., Liu, T., Doll, G.L., 2017. A fundamental study of oil release mechanism in soap and non-soap thickened greases. Tribol. Int. 110, 333–340. https://doi.org/10.1016/j.triboint.2017.02.004

Shuff, P.J., Clarke, L.J., 1991. The structure of grease via electron microscopy and image analysis. Lubr. Sci. 4, 35–50.

Tichy, J., Menut, M., Oumahi, C., Muller, S., Bou-Saïd, B., 2020. Grease flow based on a two-component mixture model. Tribol. Int.

Wikström, V., Jacobson, B., 1997. Loss of lubricant from oil-lubricated near-starved spherical roller bearings. Proc. Inst. Mech. Eng. Part J J. Eng. Tribol. 211, 51–66.

Zhang, Q., Mugele, F., Lugt, P. M., and van den Ende, D., 2020. Characterizing the fluid-matrix affinity in an organogel from the growth dynamics of oil stains on blotting paper. Soft Matter, 16(17), 4200-4209.

9 NOMENCLATURE

Index *i* stands for the components oil (O) or thickener (T).

$\varepsilon_i^G(t,z)$	Local volume fraction of component "i" in grease (G)	(-)
$\varepsilon_{T,max}^G$	Maximum volume fraction of thickener obtained when the grease is totally compressed	(-)
φ	Sieve's porosity	(-)

ρ_i	Density of the component "i"	(kg.m^{-3})
ρ_M	Density of the mass	(kg.m^{-3})
η_i	Viscosity of the component "i"	(Pa.s)
$\theta(t,z)$	Thickener fibres deviation angle with respect to z axis	rad
C_{per}^{te}	Adjustment constant for parametric estimation of the perpendicular permeability	-
C_{par}^{te}	Adjustment constant for parametric estimation of the parallel permeability	-
$f_i^G(t,z)$	Local volumetric flux density of component "i" in grease G	(m.s^{-1})
g	Gravitational acceleration	(m.s^{-2})
h	Coordinate of the moving interface of grease	(m)
$h_{BO}(t)$	Thickness of the bleeding oil film (BO)	(m)
$h_G(t)$	Thickness of the compacted grease (G)	(m)
$h_{G,min}$	Minimum grease height obtained when the grease is totally compressed	(m)
h_M	Thickness of the mass (M)	(m)
h_{Grid}	Height of the sieve grid	m
H	Hessian matrix	(-)
$k(t,z)$	Permeability of the porous network	(m²)
$k_{per}(t,z)$	Permeability associated with oil flow perpendicular to the fibres	m²
$k_{par}(t,z)$	Permeability associated with oil flow parallel to the fibres	m²
$k_\theta(t,z)$	Permeability due to fibers tilting	m²
L	Total thickness of lubricant	(m)
M_i	Total mass of the component "i"	(kg)
m_M	Mass (M) of solid	(kg)
N	Number of discretization in grease (G)	(-)
$\mathcal{P}$	Total momentum	(kg.m.s^{-1})
$P_{ambient}$	Ambient pressure	(Pa)
$P(t,z)$	Pressure	(Pa)
$P(t,L)$	Pressure on the sieve at z=L	(Pa)
$P_i^G(t,z)$	Pressure of the component "i" in grease at z (G)	(Pa)
$P_G(t,z)$	Pressure in grease at z (G)	(Pa)

r	Radius of the thickener fibres	m
R_{Grid}	Radius of the holes of the sieve grid	m
S	Total surface of the system	(m^2)
Sen	Matrix of sensitivities	(-)
t	Time	(s)
$t_{Student}$	Student variable	(-)
T	Temperature	°C or K
$V_G(t)$	Volume of grease (G)	(m^3)
$V_i^G(t)$	Volume of the component "i" in grease (G)	(m^3)
V_T	Total volume of G and OB	(m^3)
$v_i^G(t,z)$	Local velocity of the component "i" in grease (G)	($m.s^{-1}$)
$v_{grid}(t)$	Average velocity of the oil flow through the sieve (BO)	($m.s^{-1}$)
$v^M(t)$	Velocity of mass displacement	m/s
z	Coordinate in the inertial system	(m)
Δz	Step of discretization in grease (G)	(m)